

# Integrated Measurement of the Mass and Surface Charge of Discrete Microparticles Using a Suspended Microchannel Resonator

Philip Dextras,<sup>†</sup> Thomas P. Burg,<sup>†</sup> and Scott R. Manalis<sup>\*,†,‡</sup>

Departments of Biological Engineering and Mechanical Engineering, Massachusetts Institute of Technology (MIT), 20 Ames Street, Cambridge, Massachusetts 02139

Measurements of the mass and surface charge of microparticles are employed in the characterization of many types of colloidal dispersions. The suspended microchannel resonator (SMR) is capable of measuring individual particle masses with femtogram resolution. Here, we employ the high sensitivity of the SMR resonance frequency to changes in particle position, relative to the cantilever tip, to determine the electrophoretic mobility of discrete particles in an applied electric field. When a sinusoidal electric field is applied to the suspended microchannel, the transient resonance frequency shift corresponding to a particle transit can be analyzed by digital signal processing to extract both the buoyant mass and electrophoretic mobility of each particle. These parameters, together with the mean particle density, can be used to compute the size, absolute mass, and surface charge of discrete microspheres, leading to a true representation of the mean and polydispersity of these quantities for a population. We have applied this technique to an aqueous suspension of two types of polystyrene microspheres, to differentiate them based on their absolute mass and their surface charge. The integrated measurement of electrophoretic mobility using the SMR is determined to be quantitative, based on comparison with commercial instruments, and exhibits favorable scaling properties that will ultimately enable measurements from mammalian cells.

Colloidal dispersions have a broad range of technological applications, including paints, pharmaceuticals, foods, photographic emulsions, ceramics, drilling muds, inks, and photonic crystals.<sup>1–5</sup> Many of these applications require very precise control over colloidal stability and, hence, interparticle interactions, which are dependent on the physicochemical properties of the particles

themselves. Therefore, quantitative measures of particle properties (such as the size, mass, and surface charge) are often valuable, with regard to designing systems and manufacturing processes for these applications. Measurements of particle size and surface charge are routinely performed using light scattering techniques such as phase-analysis light scattering (PALS).<sup>6</sup> This technique estimates the size and electrophoretic mobility of particles by measuring their average Brownian motion and their motion in an applied electric field, respectively. While applicable to a wide variety of colloidal systems, PALS reports size and mobility values that represent averages over multiple particles. Hence, accuracy in estimating the particle's charge, which is dependent on both the size and the mobility, can suffer from errors that are made in ensemble average measurements of these two parameters, both of which may be multimodal for a complex population.

Various approaches for measuring size and electrical properties of single particles have been explored, such as the Coulter principle and mass spectrometry. Carbon nanotube-based Coulter counters are able to measure discrete-particle mobility and size, but compromises must be made between the signal-to-noise ratio (SNR) of the mobility measurement and that of the size measurement, because they have inherently different optimum orifice lengths.<sup>7</sup> Measurement of the particle charge-to-mass ratio via time-of-flight mass spectrometry has been integrated with direct charge measurement using a Faraday disk; however, because the sample must be dried, the measured charge may not accurately reflect that experienced in the desired dispersion medium for a given application.<sup>8</sup>

It has been shown recently that the mass of single nanoparticles can be measured with high precision using a suspended microchannel resonator (SMR).<sup>9</sup> With this method, particle mass is measured as the change in resonance frequency of a hollow cantilever as a suspended microparticle transits the fluid-filled microchannel running through it (see Figure 1A). The net frequency shift is proportional to the buoyant mass of the particle. In addition, as the particle travels through the cantilever, the resonance frequency of the SMR is highly sensitive to its position

\* To whom correspondence should be addressed. E-mail: scottm@media.mit.edu.

<sup>†</sup> Department of Biological Engineering.

<sup>‡</sup> Department of Mechanical Engineering.

- (1) Malmsten, M.; Lindström, A.; Wörnheim, T. *J. Colloid Interface Sci.* **1996**, *179*, 537–543.
- (2) Howe, A. M. *Curr. Opin. Colloid Interface Sci.* **2000**, *5*, 288–300.
- (3) Zhao, H.; Bhattacharjee, S.; Chow, R.; Wallace, D.; Masliyah, J. H.; Xu, Z. *Langmuir* **2008**, *24*, 12899–12910.
- (4) Comiskey, B.; Albert, J. D.; Yoshizawa, H.; Jacobson, J. *Nature* **1998**, *394*, 253–255.
- (5) Xia, Y.; Gates, B.; Yin, Y.; Lu, Y. *Adv. Mater.* **2000**, *12*, 693–713.

- (6) Miller, J. F.; Schätzel, K.; Vincent, B. J. *J. Colloid Interface Sci.* **1991**, *143*, 532–554.

- (7) Ito, T.; Sun, L.; Bevan, M. A.; Crooks, R. M. *Langmuir* **2004**, *20* (16), 6940–6945.

- (8) Peng, W. P.; Lin, H. C.; Chu, M. L.; Chang, H. C.; Lin, H. H.; Yu, A. L.; Chen, C. H. *Anal. Chem.* **2008**, *80* (7), 2524–2530.

- (9) Godin, M.; Bryan, A. K.; Burg, T. P.; Babcock, K.; Manalis, S. R. *Appl. Phys. Lett.* **2007**, *91* (12), 123121.

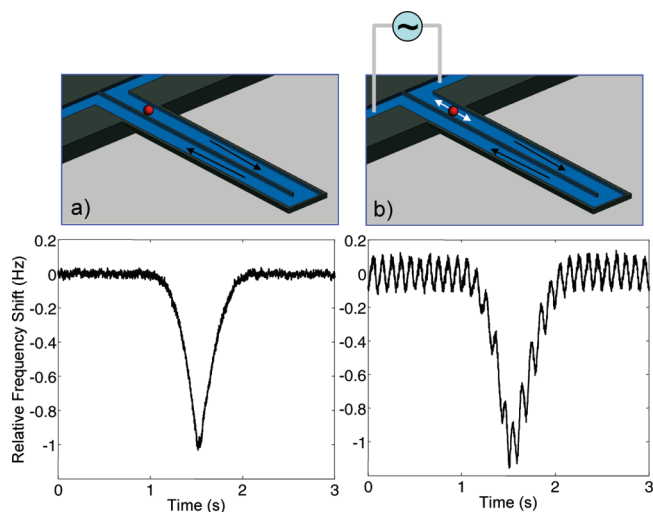


**Figure 1.** (a) Cut-away view of the fluid-filled suspended micro-channel through which particles travel (top). This channel is a tunnel through the inside of the resonant cantilever structure. A transient resonance frequency time course is shown (bottom) for a 2.2- $\mu\text{m}$  polystyrene particle that drifts through the sensor under a small pressure gradient. The height of the peak is proportional to the particle's buoyant mass. (b) If an oscillating electric field is applied longitudinally to the channel, particles will oscillate at the same frequency, because of a combination of electrophoresis and electro-osmotic flow. Spectral analysis of the resulting resonance frequency time course can be performed to extract the particle's electrophoretic mobility.

along the cantilever's length. Here, we have exploited this property to accurately quantify the electrophoretic mobility of polystyrene microspheres traveling through the SMR while being subjected to oscillatory electric fields (see Figure 1B). We demonstrate that recorded resonance frequency time courses that correspond to particles traveling through the SMR while undergoing oscillatory electrophoresis can be analyzed to extract both the particle's buoyant mass and electrophoretic mobility. Measurement of these two parameters, combined with the particle's density, allows the absolute mass and surface charge of individual particles to be computed. We have used this technique to show that integrated single-particle mass and surface charge measurement enables differentiation of complex particle mixtures that is not possible using either measurement alone.

The technique has been demonstrated by analyzing a mixture of polystyrene microspheres with nominal diameters of 1.96 and 2.20  $\mu\text{m}$  and a density of 1.05  $\text{g}/\text{cm}^3$  in SMRs with a channel height of 3  $\mu\text{m}$ . The electrophoretic mobilities of particles and the electro-osmotic mobility of the channel are estimated using the Helmholtz–Smoluchowski formula, because of their large sizes, relative to the double layer thickness, which is estimated to be 2.6 nm under the present buffer conditions. In this approximation, the particle velocity and electro-osmotic flow velocity are given by

$$v_{\text{EP}} = \frac{\varepsilon \zeta_{\text{p}} E}{\eta} \quad (1a)$$

and

$$v_{\text{EOF}} = -\frac{\varepsilon \zeta_{\text{w}} E}{\eta} \quad (1b)$$

where  $\varepsilon$  is the permittivity of the buffer,  $\eta$  the buffer viscosity,  $E$  the electric field strength,  $\zeta_{\text{p}}$  the zeta potential of the particle, and  $\zeta_{\text{w}}$  the zeta potential of the channel wall.<sup>10</sup> Because the polystyrene microspheres and the silicon dioxide channel surfaces are both negatively charged under the present buffer conditions, the electrophoretic and electro-osmotic forces on a particle oppose each other. Particles that are subjected to a sinusoidal electric field ( $E = E_0 \sin(\omega t)$ ) will oscillate with a spatial amplitude that is proportional to their relative zeta potential:

$$A = (\zeta_{\text{p}} - \zeta_{\text{w}}) \frac{\varepsilon E_0}{\eta \omega} \quad (2)$$

where the sign of the spatial amplitude ( $A$ ) indicates whether the motion is aligned with the field (positive sign) or opposed to it (negative sign). If the channel wall's zeta potential and the electric field parameters are known, then one can determine the particle's zeta potential from eq 2 by measuring the spatial amplitude. From the particle's measured zeta potential and volume, the surface charge can be estimated using the Loeb formula for a monovalent binary ionic solution:

$$Q = \pi \varepsilon \kappa a^2 \left( \frac{kT}{e_0} \right) \left[ 2 \sinh \left( \frac{e_0 \zeta_{\text{p}}}{2kT} \right) + \left( \frac{8}{\kappa a} \right) \tanh \left( \frac{e_0 \zeta_{\text{p}}}{4kT} \right) \right] \quad (3)$$

where  $a$  is the particle's diameter,  $\kappa$  the Debye–Hückel parameter,  $e_0$  the electron charge,  $kT$  the thermal energy, and  $\zeta_{\text{p}}$  the zeta potential of the particle.<sup>11</sup>

To determine the spatial amplitude  $A$ , which is described in eq 2, we model the resonance frequency of the SMR,  $f(t)$ , in response to an oscillating particle that drifts through the channel at a constant velocity  $v_{\text{d}}$ , as determined by the pressure gradient. Thus, the axial position  $x$  of the particle along the channel is given by

$$x = v_{\text{d}} t + A \sin(\omega t)$$

As the particle passes through the channel, the induced frequency shift is described by a nonlinear function,  $f(x)$ , which is zero at the base and has a maximum at the apex. Although this function is not known, we can estimate the rate of change of the resonance frequency, which is given by

$$\frac{df}{dt} = \frac{df}{dx} \frac{dx}{dt} \quad (4)$$

The first term in this chain-rule expansion corresponds to the local sensitivity of the resonance frequency to changes in particle position, whereas the second term represents the instantaneous particle velocity. Because the spatial amplitude, which is typically on the order of 10  $\mu\text{m}$ , is small, compared to the cantilever length of 200  $\mu\text{m}$ , we can approximate the first term by the value it would have in the absence of oscillation. Practically, this approximation is made by band-stop filtering the frequency time course data,

(10) von Smoluchowski, M. *Handbuch der Elektrizität und des Magnetismus*; Barth: Leipzig, Germany, 1921; Vol. 2, 366 pp.

(11) Hunter, R. J. *Zeta Potential in Colloid Science: Principles and Applications*; Academic Press: New York, 1981.

$\tilde{f}(t)$ , at the oscillation frequency. Because the position of the particle is not known, we estimate the spatial derivative by dividing the time derivative by the drift velocity:

$$\frac{df}{dx} \approx \frac{1}{v_d} \frac{d}{dt} F_{BS}[\tilde{f}]$$

The drift velocity is approximated by the baseline width of the peak in the band-stop-filtered frequency signal, and the height of the peak is used to compute the particle's buoyant mass. The calibration of the device, in terms of the proportionality between resonance frequency and added mass, has been reported elsewhere.<sup>9</sup> The second term in the expansion, the particle's instantaneous velocity, is given by

$$\frac{dx}{dt} = v_d + \omega A \cos(\omega t)$$

Substituting these expressions into eq 4 yields

$$\frac{df}{dt} \approx \left[ 1 + \left( \frac{\omega A}{v_d} \right) \cos(\omega t) \right] \frac{d}{dt} (F_{BS}[\tilde{f}])$$

A band-pass filter centered at the oscillation frequency is applied to both sides of this approximation, eliminating the low-frequency first term on the right-hand side. The order of differentiation and filtering on the left-hand side can be reversed because both operations are linear and time-invariant, which facilitates evaluation of the numerical derivative. Rearranging this relationship, in terms of the spatial amplitude, yields the following expression:

$$A = \frac{\left( \frac{v_d}{\omega} \right) \frac{d}{dt} F_{BP}[\tilde{f}]}{F_{BP} \left[ \cos(\omega t) \frac{d}{dt} (F_{BS}[\tilde{f}]) \right]} \quad (5)$$

These operations provide a practical means by which to estimate the spatial amplitude of oscillation ( $A(t)$ ) from the raw resonance frequency data ( $\tilde{f}(t)$ ).

## EXPERIMENTAL SECTION

To integrate electrophoretic mobility measurement capabilities into the SMR, modifications were needed both at the device and system level (see Figure 2). At the device level, the silicon channel walls were electrically passivated with a thermal oxide layer to support electric fields in the fluid for electrophoresis. However, this passivation oxide can break down if the cantilever is driven to resonance using the electrostatic approach that has been used previously.<sup>12</sup> Because the cantilever contains a microchannel, using the cantilever as an electrode in the drive circuit creates a large ground plane behind the walls of this microchannel, which is separated from the fluid by only the passivation oxide thickness. The need for large potential differences in the fluid to drive electrophoresis then results in large voltages being developed directly across the oxide which cause breakdown of the oxide, as observed by electrolysis of the fluid. This situation is avoided if

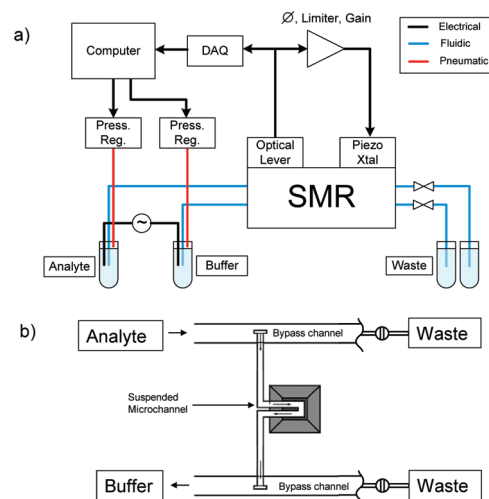


**Figure 2.** (a) Schematic diagram of the instrument. The SMR resonance frequency is measured in a feedback loop, using optical lever readout and piezoelectric actuation. The rate and direction of fluid flow through the sensor is controlled electronically (via a pair of air pressure regulators connected to two reservoirs that supply the sensor's two bypass channels) and manually (using valves at the bypass outlets). (b) Detailed schematic of the sensor. In the normal mode of operation, outlets of the bypasses are closed at the valves and reservoir pressures adjusted to determine the particle drift velocity.

the bulk silicon is allowed to float its potential to match the local fluid voltage. Therefore, in the present work, actuation was performed by means of a piezoelectric crystal external to the device (Model PL022, Physik Instrumente GmbH & Co. KG, Karlsruhe/Palmbach, Germany). This crystal's 4 mm<sup>2</sup> footprint is small enough that it can make direct contact with the device's 145 mm<sup>2</sup> bottom surface without interfering with the optical lever beam. Contact force is adjusted by means of a set screw embedded in the manifold that seals the external tubing against the device's fluid access ports on its top surface. Electrodes for electrophoresis were also integrated at the system level, to minimize complications due to electrolysis. This was accomplished using a custom manifold that incorporated both platinum wire electrodes and air pressure control elements that are needed to achieve precise control over the particle drift velocity.

**Device Passivation.** Electrical passivation of the device was accomplished by growing 800 Å of thermal oxide on all silicon surfaces that contact the fluid. Dry thermal oxide was grown at 850 °C for 15 min, followed by a 42-min wet oxidation and a 30-min dry oxidation at the same temperature. This oxide has been determined to support electric fields up to 1650 V/cm in the fluid before it breaks down and shunts current through the bulk silicon.

**Device Actuation.** Because the piezoelectric drive transducer employed here for actuating the SMR has a much higher capacitance than the micropatterned drive electrode used in the electrostatic scheme, a power amplifier stage was added to the feedback loop. A limiter truncates the optical lever output signal for input to an Apex PA-94 amplifier (Cirrus Logic, Inc., Austin, TX), the output voltage of which is divided between a current-limiting resistor and the piezoelectric crystal load. This circuit allows the highly capacitive load to be driven with sufficient

(12) Burg, T. P.; Mirza, A. R.; Milovic, N.; Tsau, C. H.; Popescu, G. A.; Foster, J. S.; Manalis, S. R. *J. Microelectromech. Syst.* **2006**, *15* (6), 1466–1476.

current to actuate the device at the resonance frequency of 183 kHz with minimal distortion of the phase.

**Material Preparation.** Dyed polystyrene particles suspended in deionized water, with nominal diameters of 2.20 and 1.96  $\mu\text{m}$ , obtained from Thermo Fisher Scientific, Inc. (Waltham, MA) and Corpuscular, Inc. (Cold Spring, NY), respectively, were resuspended together in 14 mM phosphate-buffered saline (pH 7.8) to concentrations of  $6.8 \times 10^6$  and  $2.5 \times 10^7$   $\text{mL}^{-1}$ , respectively. These concentrations were chosen to compensate for the higher nonspecific binding of the second particle type to the silicon oxide surfaces of the device channel walls, to produce approximate parity in the number of transits for the two particle types.

**Particle Measurement Protocol.** As reported previously, the mean particle density for a population can be inferred by measuring the mean particle buoyant mass in at least two media that have different densities.<sup>9</sup> Knowledge of the mean density then allows the buoyant mass measurement to be converted to either a volume or an absolute mass. In this work, particle volumes and absolute masses were computed from the measured buoyant masses using a particle density of 1.05  $\text{g}/\text{cm}^3$ , which is specified by the manufacturer. However, the instrumentation used to make the integrated measurements described here also has all the capabilities needed to measure particle density. The particle suspension was loaded into a pressurized reservoir that was connected to one bypass channel of the SMR while a reservoir supplying the other bypass channel was filled with the same buffer without particles (see Figure 2). Air pressure regulators connected to the two reservoirs and valves at the outlets of the bypass channels determined the direction and rate of flow through the sensor. For integrated measurements, both outlet valves were closed, and the regulators were adjusted to produce a flow rate of  $\sim 10$   $\text{pL}/\text{s}$  through the suspended microchannel, which corresponded to a linear particle velocity of  $\sim 400$   $\mu\text{m}/\text{s}$ . Larger velocities were determined to yield insufficient data for particle mobility measurement, whereas smaller velocities caused greater interactions between particles and the channel walls, which interfered with mobility measurement. Electrophoresis was induced by applying a sinusoidal potential with a frequency of 10 Hz and amplitude of 125  $V_p$  between electrodes that were contained in the two reservoirs.

**Determination of Electric Field.** Because the two sample reservoirs are connected to the device through tubes and valves that have unknown internal geometries, determining the electric field in the suspended microchannel required further system characterization. A Keithley Model 237 source-measure unit (Keithley Instruments, Inc., Cleveland, OH) was connected to the reservoir electrodes and averages over at least 20 current measurements made at 200 ms intervals were tabulated for 19 different voltages between 1 V and 100 V to determine the ionic conductance of the overall system. Reservoirs made from pipet tips were then connected directly to the surface of an identical device with epoxy, so that the conductance of the device alone could be measured in the same way. These two conductances were compared, to determine how voltages applied to the electrodes are divided between the device itself and tubing external to it. Because dimensions internal to the device are determined by well-characterized microfabrication processes, the

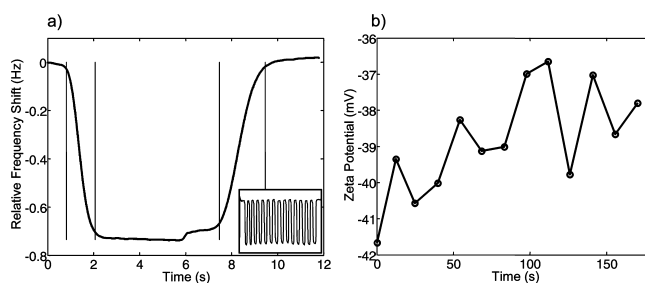


**Figure 3.** Channel wall zeta potential is measured using a bidirectional buffer exchange technique. Panel (a) shows the resonance frequency time course for a single cycle in which the more-dense buffer first replaces the less-dense buffer via forward EOF, followed by the opposite buffer exchange, which is caused by reversal of the EOF voltage. The vertical lines indicate the times at which the interface between the two buffers enters/leaves the suspended microchannel. The overall time course for the experiment (13 cycles) is shown in the inset. In panel (b), the wall zeta potential determined from the measured electro-osmotic velocities is plotted against the approximate time of measurement in the overall time course.

division of voltage between the suspended microchannel and the bypass channels could be computed from known geometries to give a quantitative figure for the electric field experienced by a particle inside the sensor. It was determined that a sinusoidal voltage of 125  $V_p$  applied to the electrodes for particle electrophoresis produced a voltage of 48.4  $V_p$  across the 828- $\mu\text{m}$ -long microchannel that connected the two bypasses, corresponding to a maximum electric field of 585  $\text{V}/\text{cm}$ .

## RESULTS AND DISCUSSION

**Channel-Wall Zeta Potential Measurement.** The zeta potential of the channel wall was determined using a bidirectional buffer exchange technique. The running buffer used to make particle mobility measurements was loaded into one reservoir, and the same buffer, diluted by 10% with deionized water, was loaded into the other reservoir. Both buffers were mixed with trace amounts of 500-nm-diameter dyed polystyrene particles (Thermo Fisher Scientific, Inc., Waltham, MA), which are too small to cause a significant resonance frequency shift but large enough to provide a visible measure of fluid flow, using a fluorescence microscope. Pressure regulators connected to the two reservoirs were adjusted to give the smallest pressure-driven flow rate possible. This was accomplished by closing the output valves of both bypasses and observing the time required for a tracer particle to travel through the suspended microchannel. When the bypass pressures were balanced, the output valves were opened to allow flow in the bypasses again and create a clean boundary between the two buffers. The output valves were then closed again and a voltage of 20 V was applied between electrodes in the two reservoirs for a time period long enough to exchange the two buffers via electro-osmotic flow. The time needed for the interface between the two buffers to travel the length of the suspended microchannel was measured as the time needed for the resonance frequency of the SMR to shift between two values corresponding to the densities of the two buffers (see Figure 3). The length of the channel divided by this transition time then provided an estimate of the electro-osmotic velocity. However, because this velocity contains a small pressure-driven component, the voltage applied to the electrodes was immediately reversed following the first buffer

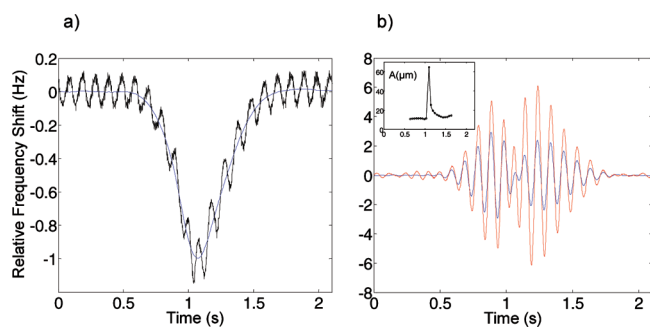


**Figure 4.** Analysis of a resonance frequency time course for the transit of a 2.2- $\mu\text{m}$  polystyrene particle subject to a 10-Hz electric field with a peak field strength of 585 V/cm. In panel (a), the raw data (black line) are filtered to separate the components of the signal due to drift and oscillatory motion of the particle. A band-stop filter recovers the drift component (blue line). The height of this peak determines the particle's buoyant mass, and its width determines the drift velocity,  $v_d$ . In panel (b), the spatial amplitude of oscillation of the particle is estimated using eq 5. Peak values of the time courses corresponding to the numerator expression (red line, shown here before scaling by  $v_d/\omega$ ) and denominator (blue line) are divided to produce the spatial amplitude time course (shown in the inset).

exchange, so that a second measurement could be made in the opposite direction. Averaging the two net velocity measurements then cancels out the effect of the pressure gradient and leaves only the electro-osmotic component. The wall zeta potential was computed from the average velocity using eqs 1a and 1b. This procedure was repeated 13 consecutive times over a period of 3 min and the results were averaged to provide an estimated wall zeta potential of  $-39.0 \pm 1.5$  mV. The trend toward lower zeta potentials is believed to be caused by diffusive mixing of the two buffers at their interface, which has a tendency to increase the time needed to register a density shift and, hence, reduces the measured electro-osmotic velocity. The variance in zeta potential measurements is most likely due to the presence of nonspecifically bound particles, which could modulate the pressure-driven component of the flow.

**Signal Processing.** The transient resonance frequency time courses that correspond to particle transits were analyzed to extract the buoyant mass and spatial amplitude of oscillation, as described previously. This analysis, as conducted using the MATLAB computing environment and illustrated in Figure 4, generally consists of computing time courses that represent the numerator and denominator expressions of eq 5 and comparing them to estimate the spatial amplitude. (Detailed algorithms used to compute particle charge and mass are given in the Supporting Information.) However, some practical issues must be considered in the application of eq 5 to the data. The resonance frequency signal exhibits a steady 10-Hz oscillation, even when the cantilever contains no particles (see Figure 4A). To eliminate this coupling, a sinusoid is fit to a baseline segment of the band-pass filtered frequency signal, and the resulting fit is subtracted from the entire time course. The phase from the fit is then used to construct the modulating sinusoid in the denominator of eq 5. Because the differentiation step in the numerator term amplifies high-frequency noise present in the raw frequency signal, a Savitzky–Golay smoothing filter is applied, in addition to the band-stop filter. The spatial amplitude is estimated by dividing local extrema of the

numerator and denominator time courses (see Figure 4B). Because the resonance frequency is not sensitive to changes in the particle's position near the cantilever's tip, the spatial amplitude exhibits a reduced SNR during this brief event. As a result, several points must be ignored in the spatial amplitude time course; however, this is acceptable for typical particle transits that last more than a second and produce over 20 measures of spatial amplitude.

**Particle Zeta Potential and Charge Measurement.** In one experiment, 51 particle transits were observed over the course of 20 min and the resulting data were analyzed to determine their spatial amplitudes and buoyant masses. These spatial amplitude data, together with the estimates of electric field and wall zeta potential described earlier, were used to compute the zeta potentials of each particle, according to eq 2, and the resulting histogram is shown in Figure 5A. To validate these measurements, suspensions of the same particles were measured using two commercial PALS-based zeta potential instruments: the Brookhaven Instruments ZetaPALS and the Malvern Zetasizer Nano ZS90 (see Figure 5B). Particles were measured at the same concentrations and under the same buffer conditions as those for the SMR, with the only difference being that the two particle types were measured separately on the commercial instruments, whereas they were measured as a mixture using the SMR. For the Brookhaven instrument, the data reported for each particle type represent the average and standard deviation of three consecutive runs, each of which is comprised of 10 PALS measurements. The corresponding data for the Malvern instrument are the result of five runs of 15 measurements. The error for the SMR measurement reflects the estimated instrument uncertainty, taking into account the standard deviations of the spatial amplitude time courses and the wall zeta potential measurements. In a separate experiment that was conducted on a different day, 101 particles were analyzed, and the difference in mean zeta potentials for the two particle types was determined to be the same (within instrument uncertainty).

Using eq 3, particle surface charge is estimated from the measured zeta potential and size for each particle. Although both the size and mass of each particle are known, the mass is a more effective parameter for differentiation, because it varies as the cube of the size and, hence, has greater resolution. Plotting the absolute masses of individual particles against their measured zeta potential or charge, as shown in Figure 6, reveals additional information about the population. Both scatter plots reveal two subpopulations of the more negative of the two particle types, which is not evident in the zeta potential data alone. We interpret these to be monomers and dimers of this particle type, because one subpopulation has a mean mass that is approximately double that of the other one at the same zeta potential. The observation that this type of particle has a tendency to aggregate more than the other type in the mixture is supported qualitatively by the observation that these particles exhibited higher nonspecific binding to the channel walls. The mass-charge scatter plot illustrates how these subpopulations are more readily differentiated on the basis of charge. This feature results from the fact that the more massive dimer particles also possess a larger net charge, which is consistent with their larger surface area. Although in the case of our two chosen particle types, there are three distinct subpopu-

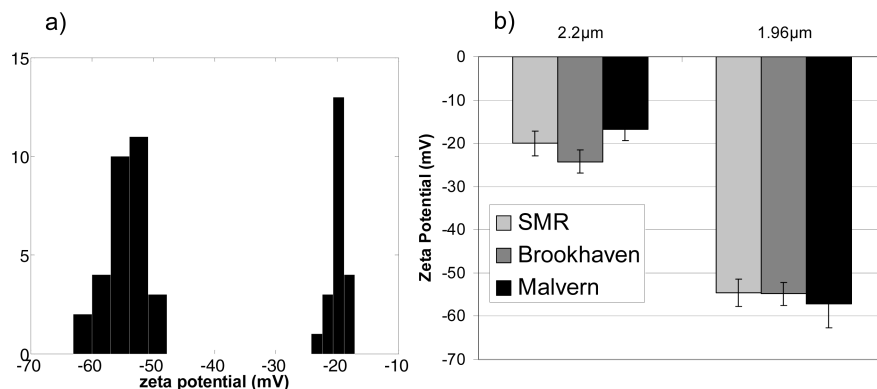


**Figure 5.** (a) Histogram of 51 single-particle zeta potential measurements made on a mixture of 2.20- and 1.96- $\mu\text{m}$  polystyrene particles using the SMR. (b) Mean zeta potentials measured for the two particle types using the SMR and two commercial instruments.

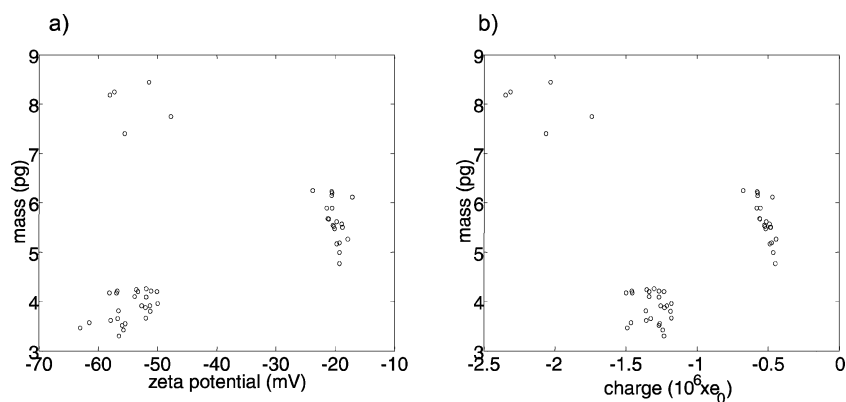


**Figure 6.** Scatter plot of the absolute mass of 51 particles from a mixture of 2.20- and 1.96- $\mu\text{m}$  polystyrene particles versus (a) their zeta potential and (b) their electrokinetic surface charge, as computed by eq 3.

lations in the mass data alone, the potential for overlap in this dimension is evident. For example, if the mean mass for the more neutral of the two particle types had been approximately double that of the more negative type, it would have obscured the dimer subpopulation for that type. Therefore, it is expected that integrated measurement of both the surface charge and mass distributions will provide advantages in the differentiation of complex particle mixtures.

The SNR of the mobility measurement technique described here is inherently dependent on the mass of the particle being measured. This can be seen from eq 4, in that a larger mobility signal, as measured by the total rate of change of the resonance frequency, can be obtained either by increasing the first term in the expansion, which is proportional to particle mass, or the second term, which is proportional to the particle's relative zeta potential. The uncertainty in position for particles of the type examined here, computed as the length of the cantilever divided by the SNR of the net frequency shift, is  $\sim 2 \mu\text{m}$ . Because these particles have typical spatial oscillation amplitudes of  $10 \mu\text{m}$ , the SNR for the spatial amplitude is on the order of 5. This is the limiting source of error in the measurement of mobility, because the SNR for the electro-osmotic mobility measurement is an order of magnitude larger. Because mass is proportional to the cube of diameter, the SNR for the mobility measurement decreases rapidly for smaller particles, if all other parameters are held constant. Furthermore, the system is physically limited by the small dimension of the suspended microchannel, which is  $3 \mu\text{m}$  in the current device. As the size of particles approaches this

value, it is expected that interactions with the channel walls will begin to dominate their trajectory through the sensor, preventing accurate mobility quantitation. On the other hand, the SNR of both mass and mobility improve if particles of greater density are examined. For example, gold nanoparticles as small as 300 nm and silica nanoparticles as small as 900 nm could be detected with the same SNR as the 2.2- $\mu\text{m}$  polystyrene particles described here, assuming that they possess the same electrophoretic mobility.

The throughput of the technique is currently limited by the algorithm used to extract the mobility from the raw data. The curve fit to the oscillatory background signal requires a window of 1 s just prior to a particle transit, during which no particles are present inside the sensor. As a result, particle concentrations were kept low so that this analysis could be performed in an automated fashion without errors. Elimination of this background signal could theoretically increase the particle throughput to its current SNR-limited value of 1 Hz. Another limitation on throughput results from the settling of particles. A certain amount of time is needed to adjust the system to achieve a flow rate through the device suitable for mobility measurement. During this time, the concentration of particles in the reservoirs decreases considerably, because of settling, sometimes reducing the throughput of particles below the desired level.

## CONCLUSIONS

We have demonstrated that the suspended microchannel resonator (SMR) provides a means of quantitatively differentiating mixed aqueous suspensions of polystyrene microspheres on the

basis of particle mass and electrokinetic surface charge. Because the technique measures individual particles, it has the potential to provide information that is obscured by other techniques that are based on ensemble average measurements. Furthermore, knowledge of both the mass and charge of individual particles in a complex mixture allows them to be more effectively differentiated than either parameter by itself.

The present instrument is based on an SMR device that is limited to particles that have diameters of  $<3 \mu\text{m}$ . However, a manufacturing process for devices that have a channel height of  $15 \mu\text{m}$  is currently being investigated. Although larger devices would suffer from decreased mass sensitivity, this effect would be more than offset by the gain in added mass for larger particles. For example, the spatial resolution of a mammalian cell with a size similar to the channel height in this new device is expected to be as low as a few tens of nanometers. In addition, as the oxide passivation process is refined to produce thicker films having higher uniformity, larger electric fields could potentially be supported. These changes and the corresponding increases in the SNR for mobility measurement will provide new opportunities, such as the ability to measure particle mobility under physiological buffer conditions, which, in turn, will allow biological specimens such as cells to be measured. We also intend to investigate the possibility of moving a single cell through the SMR multiple times

using an additional electric field component, which would allow the surface charge of the cell to be monitored as a function of time.

#### **ACKNOWLEDGMENT**

We acknowledge financial support from the National Cancer Institute Platform Partnership Grant (R01-CA119402) and the Institute for Collaborative Biotechnologies from the U.S. Army Research Office. We also acknowledge Omar Fisher from the research group of Professor Robert Langer at MIT for assistance with their BIC ZetaPALS and the research group of Professor Sangeeta Bhatia at MIT for the use of their Malvern ZetaSizer Nano ZS90.

#### **SUPPORTING INFORMATION AVAILABLE**

Detailed examinations of the algorithms that have been described in the manuscript for use in signal processing. (PDF) This information is available free of charge via the Internet at <http://pubs.acs.org>.

Received for review March 10, 2009. Accepted April 23, 2009.

AC9005149